Journal of Chromatography A 1706 (2023) 464240

Contents lists available at ScienceDirect

Journal of Chromatography A

journal homepage: www.elsevier.com/locate/chroma

Low-frequency electrokinetics in a periodic pillar array for particle separation

Víctor Calero [a,b], Raúl Fernández-Mateo [c], Hywel Morgan [c], Pablo García-Sánchez [a,*], Antonio Ramos [a]

[a] Depto. Electrónica y Electromagnetismo, Facultad de Física, Universidad de Sevilla, Avda. Reina Mercedes s/n, 41012, Sevilla, Spain
[b] International Iberian Nanotechnology Laboratory (INL), Braga 4715-330, Portugal
[c] School of Electronics and Computer Science, University of Southampton, Southampton SO17 1BJ, United Kingdom

ARTICLE INFO

Dataset link: https://doi.org/10.5258/SOTON/D2730

Keywords:
Deterministic Lateral Displacement
Particle sorting
Electrokinetics
Microfluidics
Concentration Polarisation Electroosmosis

ABSTRACT

Deterministic Lateral Displacement (DLD) exploits periodic arrays of pillars inside microfluidic channels for high-precision sorting of micro- and nano-particles. Previously we demonstrated how DLD separation can be significantly improved by the addition of AC electrokinetic forces, increasing the tunability of the technique and expanding the range of applications. At high frequencies of the electric field (>1 kHz) the behaviour of such systems is dominated by Dielectrophoresis (DEP), whereas at low frequencies the particle behaviour is much richer and more complex. In this article, we present a detailed numerical analysis of the mechanisms governing particle motion in a DLD micropillar array in the presence of a low-frequency AC electric field. We show how a combination of Electrophoresis (EP) and Concentration-Polarisation Electroosmosis (CPEO) driven wall-particle repulsion account for the observed experimental behaviour of particles, and demonstrate how this complete model can predict conditions that lead to electrically induced deviation of particles much smaller than the critical size of the DLD array.

1. Introduction

Over the last decades, there has been an increased interest in the development of microfluidic particle separation techniques. Low-volume high-precision fractionation methods are important for the development of devices capable of performing full analytical processes on a single platform. Examples include the isolation, detection and monitoring of a wide range of bioparticles (such as circulating tumour cells (CTCs), bacteria or extracellular vesicles [1–4]) from complex samples that ultimately enable early diagnosis and monitoring of disease.

Deterministic Lateral Displacement (DLD) is a promising microfluidic separation approach that delivers high-resolution continuous-flow size-based separation of particles over a wide range of sizes, from nanoparticles to cells that are tens of micrometres in size [5,6]. DLD devices take advantage of laminar flow on the microscale to sort particles in a deterministic way based on a specific geometry of an array of micro-pillars. In the DLD geometry each row of posts is displaced a given distance ($\Delta\lambda$) from the previous, defining a periodicity P given by:

$$P = \frac{\lambda}{\Delta\lambda} \tag{1}$$

where λ is the distance between consecutive rows of pillars. Fig. 1 shows a diagram of the typical DLD pillar array geometry and the physical mechanism responsible for size-based separation. The shift in the consecutive rows gives rise to a separatrix streamline which divides the fluid flow into portions passing above and below the next post. If a particle is bigger than the minimum distance from the separatrix to the nearest post, upon interaction with this post, it will be displaced towards the portion of fluid passing above the following post. As a result, particles follow the deviation angle defined by the array geometry ($\theta_D = \arctan(1/P)$), bumping on the posts and displacing laterally (dark particles in Fig. 1). If on the contrary, the particle is smaller than the distance from the separatrix to the post, it is not displaced by the posts and will remain in the fluid passing below the next post, following an

* Corresponding author.
E-mail address: pablogarcia@us.es (P. García-Sánchez).

https://doi.org/10.1016/j.chroma.2023.464240
Received 18 April 2023; Received in revised form 18 July 2023; Accepted 23 July 2023
Available online 28 July 2023

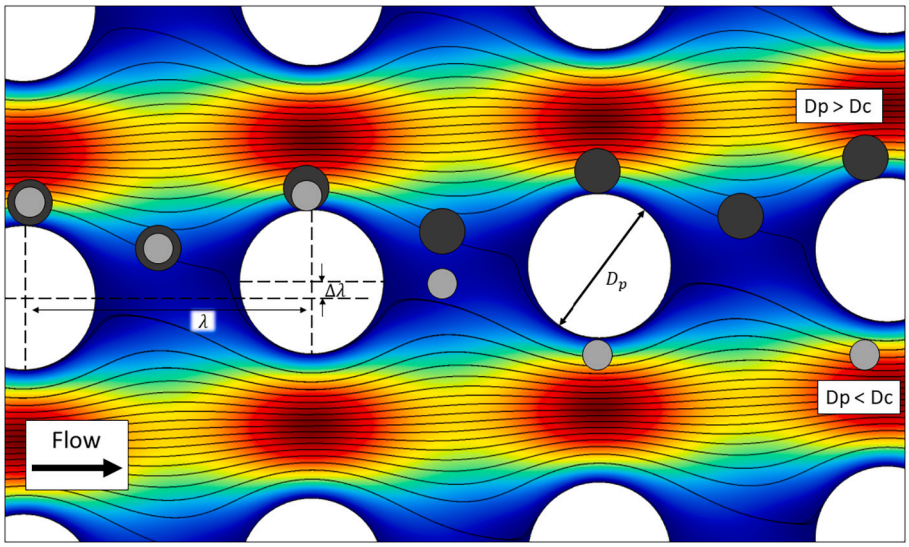

Fig. 1. Diagram representing a typical DLD cylindrical pillar array geometry. The passive size-based separation mechanism relies on the separatrix streamline which divides the flow passing above and below the following post. Particles bigger than a critical diameter D_c are displaced by the posts periodically while particles smaller follow the streamlines in an overall straight trajectory. The colour map represents the magnitude of the fluid velocity. (For interpretation of the colours in the figure(s), the reader is referred to the web version of this article.)

overall straight trajectory with zero net lateral displacement, zigzagging around the pillars (light coloured particles in Fig. 1). The critical diameter (D_c) is thus defined as the diameter above which the particles follow deviating trajectories and is therefore determined by the width of the separatrix near the posts. For a more detailed description of this mechanism see [7].

Since first reported by Huang et al. [8], DLD separation has been extensively studied and enhanced. A particularly interesting and promising approach consists of coupling DLD with external fields, turning passive DLD size-based separation into active and tunable sorting that can target additional physical properties of the particles rather than size. Amongst the many options, coupling DLD with electric fields has proven to be a very useful approach with a rich number of physical mechanisms leading to enhanced particle separation. This approach was first reported by Beech et al. [9], applying an AC electric field along the DLD channels in the direction parallel to the fluid flow. They showed tunable separation of 3 μm and 5 μm diameter particles inside a DLD device with 6 μm critical diameter, and attributed the induced deviation to Dielectrophoresis (DEP). Later [10] they showed that the particle behaviour is much richer than first claimed and explored how the deviation depended on the suspending electrolyte conductivity, the particle charge and the electric field frequency.

In recent articles, we explored the induced deviation of particles smaller than the D_c when an AC electric field is applied orthogonal to the fluid flow [11,12]. We first characterised the particle behaviour and induced separation of 500 nm, 1 μm and 3 μm in a DLD with a D_c of 6.3 μm as a function of the electric field frequency. Two different regimes were identified. At high frequencies (> 1 kHz), particle behaviour was dominated by DEP whereas at low frequencies other mechanisms came into play. The scaling laws governing the electrokinetic induced behaviour at both, high and low frequencies were explored. It was demonstrated that negative DEP (nDEP) drove the separation at high frequencies, and good agreement was found between the experimental results and numerical simulations. At low frequencies dependence of the separation was characterised as a function of the magnitude of the electric field, particle size and fluid velocity. A full theoretical model was not available at the time to account for the observations.

In this paper, we present a thorough and detailed numerical study of the low-frequency AC electrokinetic behaviour of the particles within a DLD pillar array. The model considers the low-frequency oscillating Electrophoresis (EP) along the electric field lines around the pillars together with wall-particle repulsion that occurs during EP [13–15]. We recently described the latter mechanism as driven by stationary electroosmotic (EO) flows around the particles due to Concentration-Polarization (CP) of the electrolyte surrounding the particle, termed CPEO [16,17]. The results are in excellent agreement with the observed experimental trends. This last analysis completes the understanding of the electrokinetic behaviour of particles inside the DLD devices and provides a full theoretical framework to explain the electrokinetic biased DLD particle separation.

2. Theory

2.1. High frequency regime ($f \gtrsim 1$ kHz)

Fig. 2 shows a diagram of the two different regimes of AC electrokinetic induced deviation in a DLD channel for high and low frequencies of the electric field. At high frequencies, the DEP force dominates the particle behaviour. The force arises from the spatial gradient in the electric field due to the insulating pillars (see Fig. 2a). The time average DEP acting on a particle subjected to an AC field [18,19] $\mathbf{E} = \mathrm{Re}[\mathbf{E}_0(\mathbf{r})e^{i\omega t}]$ is given by:

$$\mathbf{F}_{\mathrm{DEP}} = \pi a^3 \varepsilon \mathrm{Re}[f_{CM}]\nabla|\mathbf{E}_0|^2 \tag{2}$$

where a is the particle radius, ε the medium permittivity, f_{CM} is a complex parameter known as the Clausius-Mossotti factor and Re[...] denotes the real part of the function between brackets. The parameter f_{CM} relates the polarisabilities of the particle and the surrounding medium. When a particle is less polarisable than the medium, $\mathrm{Re}[f_{CM}] < 0$ it experiences nDEP, i.e. it is repelled from high electric field regions. When this occurs in the DLD shown in Fig. 2a, the particles are repelled from the downstream gaps between the posts. If the nDEP repulsion is strong enough to disrupt the particle trajectories and make them cross the separatrix streamline, the particles are therefore prevented from zigzagging between the posts and are forced to follow a deviating trajectory. Under the influence of a DEP force and a fluid velocity field $\mathbf{v}_f$, the particle velocity $\mathbf{u}$ is given by:

$$\mathbf{u} = \mathbf{v}_f + \mathbf{u}_{\mathrm{DEP}} \tag{3}$$

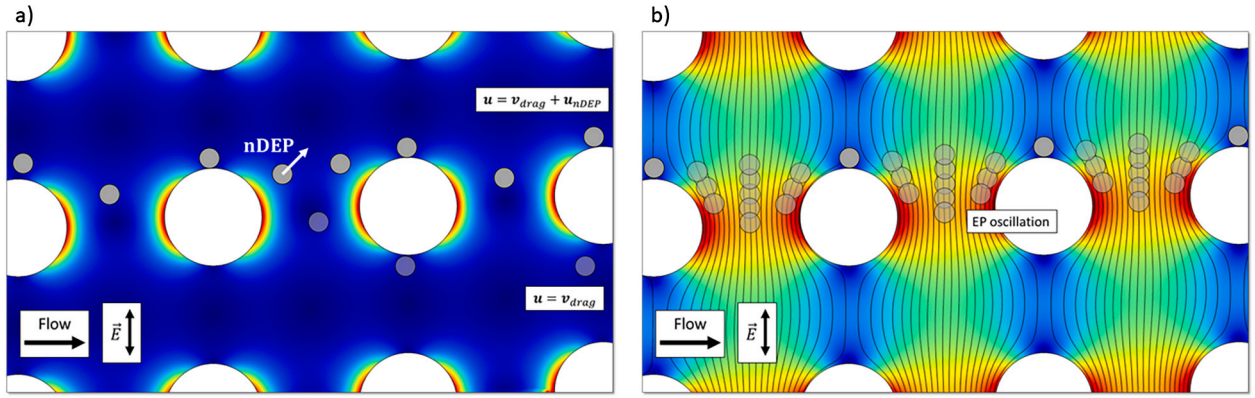

Fig. 2. Diagram of electrically tuned DLD separation. (a) Negative DEP induced separation - Colour map represents the intensity of the nDEP force. (b) Low frequency separation - Colour map represents the magnitude of the electric field.

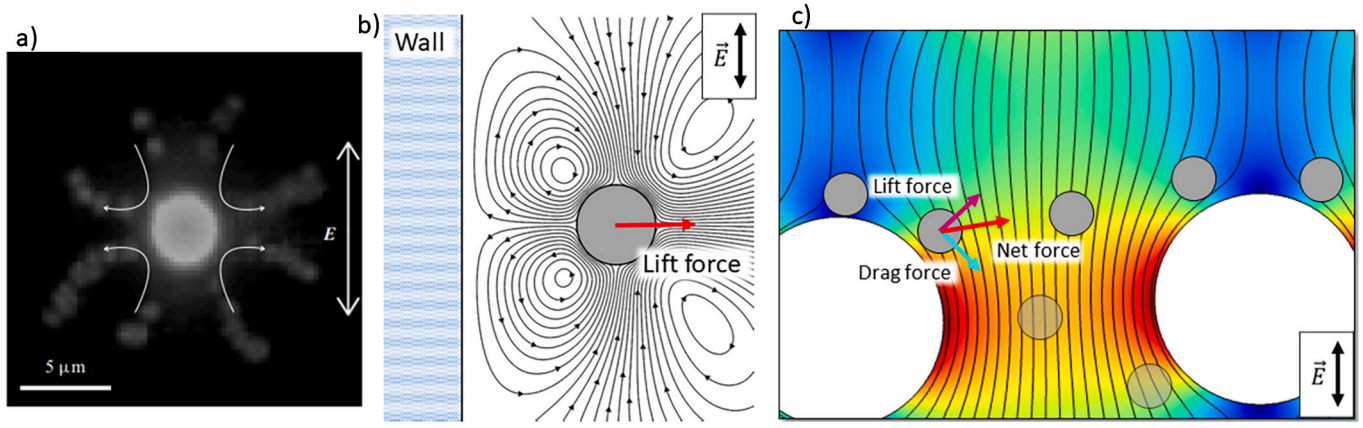

Fig. 3. Principles of CPEO assisted particle deviation in DLD arrays. (a) Experimentally observed CPEO flows around a 3 µm carboxylate particle ($f = 282$ Hz and $E = 80$ kV/m) using 500 nm fluorescent spheres as flow tracers. Reproduced from Fernández-Mateo et al. [16] (with permission from Cambridge University Press 2021). (b) Particle repulsion from a flat wall induced by CPEO flows around the particles. (c) Deviation inside DLD post array induced by CPEO wall repulsion - Colour map represents the magnitude of the electric field.

with $\mathbf{u}_{\mathrm{DEP}} = \frac{a^2 \varepsilon \mathrm{Re}[f_{CM}]}{6\eta} \nabla |\mathbf{E}_0|^2$, where η is the dynamic viscosity of the fluid. Following the analysis in Calero et al. [12], a dimensionless expression of equation (3) can be derived using the post radius R, a typical fluid velocity U, and a typical electric field magnitude E_0:

$$\tilde{\mathbf{u}} = \tilde{\mathbf{v}}_f + \mathrm{sgn}(\mathrm{Re}[\tilde{f}_{CM}]) N \tilde{\nabla} |\tilde{\mathbf{E}}_0|^2 \tag{4}$$

where the tilde indicates dimensionless magnitudes. In this equation, the dimensionless parameter $N = \frac{\varepsilon E_0^2 a^2}{6\eta R U} |\mathrm{Re}[f_{CM}]|$ quantifies the relative contribution of the DEP force to the net particle velocity, and therefore the deviation induced by this force scales with the magnitude of this parameter.

2.2. Low frequency regime ($f \lesssim 1$ kHz)

For frequencies below ~1 kHz, other forces come into play. Although the oscillating EP has a zero time-average displacement, it leads to an oscillation of the particle along the electric field lines (see Fig. 2b), with a velocity $\mathbf{u}_{\mathrm{ep}}$ given by the Helmholtz-Smoluchowski equation:

$$\mathbf{u}_{\mathrm{EP}} = \frac{\varepsilon \zeta}{\eta} \mathbf{E} \tag{5}$$

where ζ is the zeta potential of the particle [20]. We hypothesize that this oscillation leads to a pronounced interaction between the walls of the DLD posts and the finite-sized rigid particles as they flow along the microchannels, creating an induced deflection.

However, low-frequency EP is not the only phenomenon that is present at low frequencies. We recently reported the presence of Concentration-Polarization Electroosmotic (CPEO) flows around charged dielectric particles subjected to low-frequency AC electric fields [16]. The particle surface conductance leads to a perturbation in the local electrolyte concentration, and therefore in the electroosmotic slip velocity at the particle surface, creating a stationary quadrupolar flow pattern, as shown in Fig. 3a. The fluid velocity field was derived by Gamayunov et al. [21] and is given by:

$$\mathbf{v}_{\mathrm{CPEO}} = v_0 \left(\frac{(1-(r/a)^2)(1+3\cos 2\theta)}{2(r/a)^4} \hat{r} + \frac{\sin 2\theta}{(r/a)^4} \hat{\theta} \right) \tag{6}$$

where r is the distance to the particle centre and θ is the angle with respect to the flow symmetry axis, which coincides with the direction of the applied electric field. The parameter v_0 is the maximum slip velocity at the particle surfaces and scales with the electric field magnitude squared [16], $v_0 = \frac{\varepsilon a E_0^2}{\eta} \tilde{v}_0(f, \zeta, a, \ldots)$. As a result, the CPEO flows have a non-zero time average velocity with a quadratic dependence on the electric field magnitude. Their magnitude decreases with electrolyte conductivity and AC field frequency and increases with the particle surface charge. A complete theoretical description of this mechanism can be found in [16].

In a previous publication [15] we demonstrated that CPEO flow is the dominant mechanism that creates the observed particle-wall repulsion during Electrophoresis of charged dielectric particles. Our results show that the hydrodynamic interaction due to CPEO flows overcomes the DEP forces in the low frequency regime and that the latter can only explain the observed particle-wall separation at high frequencies. In the presence of a low frequency AC electric field and with the particle situ-

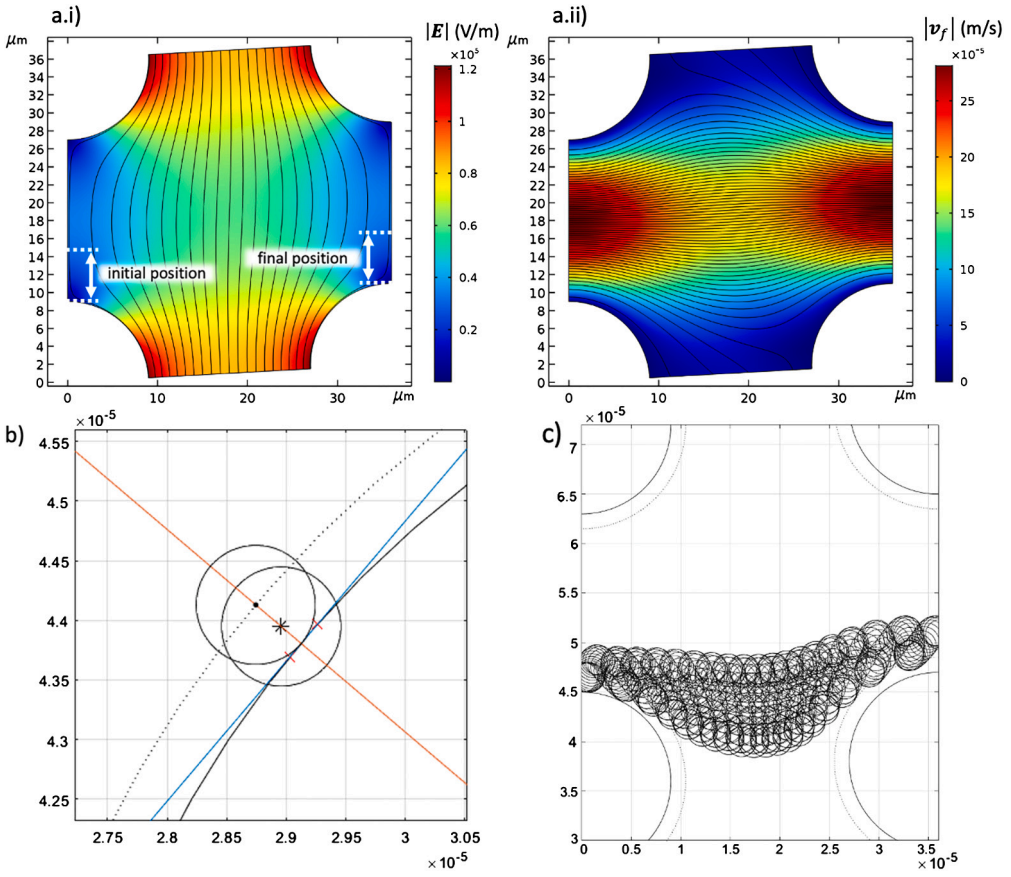

Fig. 4. (a.i) Electric field distribution calculated in the DLD unit cell, marking the initial and final position of the particles. (a.ii) Fluid flow profile inside the DLD unit cell. (b) Hard wall inelastic-collision correction. The initial position (marked with an asterisk in the particle centre) is corrected for the distance of the overlap between particle and post, to the position marked with a dot in the particle centre. (c) Example trajectory of the deviation of a 3 μm particle at low frequencies induced by CPEO and EP oscillations.

ated in the vicinity of a wall, the CPEO flow patterns become distorted, as shown in Fig. 3b. This hydrodynamic interaction gives rise to a net particle velocity with respect to the nearby wall which can be calculated following the method of reflections [22]. For the case of an electric field parallel to the wall, there is a net particle repulsion perpendicular to the wall given by [23,24]:

$$\mathbf{u}_{\text{rep}} = v_0 \frac{3a^2}{8h^2}\hat{z} \tag{7}$$

where h is the distance from the particle centre to the wall and $\hat{z}$ the unit vector which is perpendicular to the wall. The constant v_0 is the CPEO slip velocity at the surface of the particle [16]. This is the leading-order term in the method of reflections for small values of a/h. A similar analysis can be used to predict the particle velocity perpendicular to the wall for the case of an electric field perpendicular to the wall. In this case, the CPEO flow leads to wall-particle attraction with a velocity given by [24]:

$$\mathbf{u}_{\text{at}} = -v_0 \frac{3a^2}{4h^2}\hat{z} \tag{8}$$

Smart and Leighton [24] also showed that, when the field is at an angle to the surface of the flat wall ($0 < \varphi < \pi/2$), there is an extra component to the particle velocity, that is tangential to the wall given by:

$$\mathbf{u}_{\text{tan}} = -v_0 \frac{3a^2}{4h^2} \sin\varphi\cos\varphi\hat{x} \tag{9}$$

A detailed derivation of these equations can be found in the supplementary material.

In this paper, we describe the role of this mechanism in a DLD array as particles are repelled from the posts. We hypothesize that the CPEO particle-wall repulsion plays a major role in the low-frequency electrokinetic-induced deviation. Every time a particle approaches a DLD pillar, the hydrodynamic interaction leads to particle repulsion from the pillar. If this repulsion is strong enough, then particles are forced to switch from a zigzagging trajectory to the displacement mode, following the array deviation angle (see Fig. 3c).

3. Numerical methods

3.1. High frequency regime simulations

At high electric field frequencies, the only forces acting on the particles are the hydrodynamic drag force from the net fluid flow along the microfluidic channels and DEP. To simulate this situation we followed the exact same methods previously described by Calero et al. [12]. The spatial distribution of the electric field and fluid flow velocity is first calculated inside a DLD unit cell (see Fig. 4a) using Finite Element Analysis and the software COMSOL Multiphysics v5.4. To calculate the fluid flow, the 2D Stokes equation ($Re \sim 10^{-3}$) was solved with periodic boundary conditions in the perpendicular and longitudinal directions, enforcing a zero net velocity in the direction perpendicular to the flow and mean fluid velocity magnitude of $U = 100$ μm/s in the longitudinal direction. A no-slip boundary condition was used at the surface of the posts. The electric field $\mathbf{E}$ was calculated from the perturbation $\mathbf{E}'$ of a uniform field $E_0\hat{y}$. For the case of an electric field in the direction y (perpendicular to the fluid flow):

$$\mathbf{E} = \mathbf{E}' + E_0\hat{y} \rightarrow \phi = \phi' - E_0 y \tag{10}$$

Thus, to calculate $\mathbf{E}'$ the Laplace equation was solved for the electrical potential ϕ' with periodic boundary conditions at the boundaries of the unit cell. To model the pillars as insulators the following condition was used at the surface of the posts:

$$\frac{\partial \phi}{\partial n} = 0 \rightarrow \frac{\partial \phi'}{\partial n} = E_0 n_y \tag{11}$$

where n_y is the y-component of a unit vector normal to the boundary.

Fig. 4a shows the spatial dependence of the fluid velocity and electric field magnitude in the DLD unit cell. The trajectories of more than 2000 particles inside a DLD unit cell were simulated for different initial positions equally distributed and covering the entire possible range, with the velocity given by equation (3).

The initial and final positions (as defined in Fig. 4a.i) are related by a transfer function which can then be used to calculate, using linear interpolation, the final position of any particle entering the unit cell for any value of initial position [12,25]. The transfer function will thus depend on the ratio between the fluid drag force and the DEP force and can be used to estimate the deviation angle after a particle crosses a large number of unit cells. In every iteration, a particle in deviation mode exits the unit cell at the same distance from the nearest post at which it entered. This is then reflected in the transfer function by crossing the line of slope 1 that passes through the origin, i.e. in the trajectory across the unit cell the initial and final positions (as defined in Fig. 4a.i) are equal.

In this study we used parameters that enabled comparison with the experimental results [12]: $U = 100\mu$m/s, $\mathrm{Re}[\tilde{f}_{CM}] = -0.5$, $a = 0.5, 1.5\mu$m and $|\mathbf{E}_0| < 80$kV/m and with a symmetric DLD geometry with $D_p = \lambda/2$ and $P = 18$ ($\theta = 3.18°$). The particle-wall interaction was modelled as a non-elastic hard wall collision as described by Kim et al. [25] and in our previous work [12]. Briefly, we considered an exclusion zone of one particle radius around the posts. Thus particles with an initial/final position closer than a to a post were considered to enter/exit the unit cell at a distance a from that post. In the transfer function, this translates into removing the prohibited initial and final (exit) positions from this function [12].

3.2. Low-frequency regime simulations

In the low-frequency regime, the approach used for high frequencies is not valid because of the significant electrophoretic oscillation of particles. This introduces an extra degree of complexity through the addition of a new parameter, the phase of the electric field. This is because the phase of the field with which the particle enters the unit cell differs from the exiting phase, depending on the time the particle takes to cover the distance of the unit cell. This adds an extra dimension to the numerical simulations and turns the 1D-1D transfer function into a 2D-2D function. The supplementary material includes a diagram of the workflow followed for the simulation procedure for both cases (high and low frequencies).

To circumvent this complexity, a different approach was taken by simply simulating the trajectories of a single particle after it has crossed a large number of unit cells. To realise this the electric and fluid fields were exported to MATLAB R2022b and the particle trajectories were calculated across a large number of unit cells (360 unit cells, i.e. 20 periods of the DLD array), until the trajectory converged into either a zig-zag or displacement mode. The components of the particle velocity are:

$$\mathbf{u} = \mathbf{v}_f + \mathbf{u}_{\mathrm{EP}} + \mathbf{u}_{\mathrm{rep}} + \mathbf{u}_{\mathrm{at}} \tag{12}$$

For simplicity the tangential component $\mathbf{u}_{\mathrm{tan}}$ (given by equation (9)) was not considered in the simulations since this component is much smaller than the electrophoretic velocity ($\mathbf{u}_{\mathrm{ep}} \gg \mathbf{u}_{\mathrm{tan}}$). The EP velocity $\mathbf{u}_{\mathrm{ep}}$ is given by equation (5), which for an oscillating field with angular frequency ω and phase φ, $\mathbf{E} = \mathbf{E}_0 \cos(\omega t + \varphi)$, produces an oscillating motion along the electric field lines, only relevant for low values of ω. The values for ζ were measured experimentally and used as input to the model: $\zeta = -70$ mV and $\zeta = -78$ mV for the 1 μm and 3 μm diameter particles, respectively. Since in this case the electric field is neither tangential nor perpendicular to the pillar wall, to calculate the contribution of the CPEO hydrodynamic interaction $\mathbf{u}_{\mathrm{rep}}$ and $\mathbf{u}_{\mathrm{at}}$ were calculated at each point of the unit cell as:

$$\mathbf{u}_{\mathrm{rep}} = \upsilon_0 \frac{3a^2}{8h^2} \frac{|E_t|^2}{|E_0|^2} \hat{n}, \tag{13}$$

$$\mathbf{u}_{\mathrm{at}} = -\upsilon_0 \frac{3a^2}{4h^2} \frac{|E_n|^2}{|E_0|^2} \hat{n}, \tag{14}$$

where E_t and E_n are, respectively the tangential and normal components of the electric field to the pillar wall at the particle position and $\hat{n}$ a unit vector perpendicular to the wall [26]. The value for υ_0 is the only input to the model and was estimated experimentally following the methods described by Fernandez-Mateo et al. [15], where the wall-repulsion was measured along a straight channel with the electric field applied parallel to the fluid flow. This was done in conditions that allowed comparison to published experimental data [12] (at an electrolyte conductivity of 2.8 mS/m, an electric field of 50 Hz and 60 kV/m, and particle diameters of 1 and 3 μm): $\upsilon_0 = (109.4 \pm 18.6)$ μm/s for 1 μm particles and $\upsilon_0 = (324.5 \pm 25.0)$ μm/s for 3 μm particles. In order to estimate υ_0 for other electric field magnitudes, the measurements at 60 kV/m were used together with the quadratic dependence with $|E|$ predicted by the CPEO model [16]. This model also allows to predict a theoretical value for υ_0 from the particle/medium properties and the electric field magnitude and frequency, but measuring υ_0 experimentally allows a more accurate comparison with our numerical model.

Finally, the particle-wall interaction was modelled as a hard-wall inelastic collision. At each time step, if a particle approached the post boundary at a distance smaller than a particle radius, the particle position was corrected the same distance in the direction perpendicular to the wall. An example of this correction is given in Fig. 4b. A typical trajectory of a 3 μm particle across a DLD unit cell under the influence of a low-frequency electric field ($E_0 = 20$ kV/m and $f = 50$ Hz), i.e. EP and CPEO wall interaction is shown in Fig. 4c.

With this model we are replicating the experimental design described in Calero et al. [12] where the devices were pretreated with a surfactant (Pluronic F-127) to avoid particle adhesion and minimize electroosmotic flow [27–29]. Consequently, in the simulations the low frequency oscillations are solely caused by electrophoresis. Also note that CPEO flows around the insulating posts are not considered ([12,30]) due to the fact that the post diameter is larger than the height of the microchannels. Since the upper and lower walls are very close, the no-slip condition significantly reduces the magnitude of these flows. Finally, for simplicity, we have assumed in this regime that the DEP contribution is negligible with respect to the contributions of EP and CPEO. This assumption is supported by experimental data where the low-frequency deviation is demonstrated regardless of the DEP behaviour of the particles: induced deviation was observed not only for nDEP particles but, also, for particles with positive DEP (pDEP) or with $\mathrm{Re}[\tilde{f}_{CM}] \sim 0$. Numerical data in the results section validate this simplification.

4. Results

4.1. Simulation results and comparison with experimental data

To test the model, the dependence of the deviation angle for 1 μm and 3 μm diameter rigid spheres was analysed as a function of the applied electric field magnitude, at high and low frequencies for an electric field applied perpendicular to the fluid flow. We then compared the results with the experimental data previously reported [12]. The results are summarised in Fig. 5. The deviation angle is directly calculated

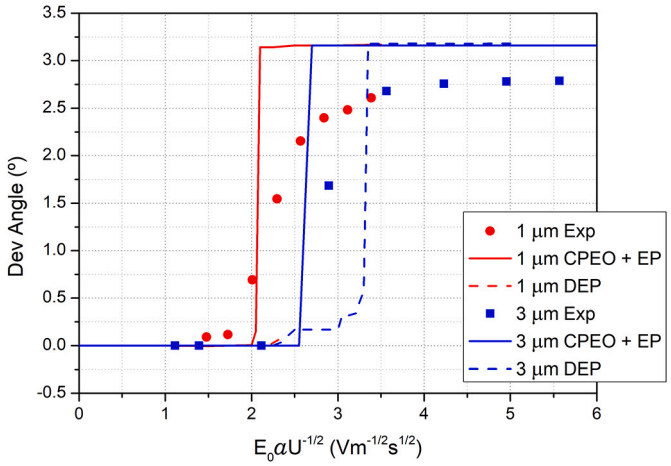

Fig. 5. Comparison of experimental data for 1 µm and 3 µm particles with simulations results: (electrolyte conductivity of 2.8 mS/m and field frequency of 50 Hz) at low frequencies including EP oscillation and CPEO wall interaction (solid lines) and high frequencies with nDEP (dashed lines). Note that the simulation results for the high-frequency deviation of 1 µm and 3 µm collapse and overlap.

from the net lateral displacement given by the simulations, and is plotted against the ratio $E_0 a/\sqrt{U}$, to enable a direct comparison between all data sets (with different values of U and particle sizes). This is valid since it is the ratio between the quadratic electric forces and the hydrodynamic drag from the fluid flow. This leads to an overlapping set of curves for the nDEP induced deviation. Note that the simulations at high frequencies assume $\mathrm{Re}[\tilde{f}_{CM}] = -0.5$, i.e. the nDEP magnitude is maximum and therefore nDEP induced deviation is also maximum. For the experimental conditions at which the deviation and the parameter v_0 were measured, the nDEP is even weaker for the 3 µm particles with $\mathrm{Re}[\tilde{f}_{CM}] = -0.21$ or is even positive DEP for the 1 µm particles with $\mathrm{Re}[\tilde{f}_{CM}] = 0.12$.

The figure shows that at low frequencies the results from the model (including contributions from EP oscillation and CPEO) match the experimental trends. It predicts a clear difference in the critical electric field, i.e. the value of $|E_0|$ at which the particles switch to the displacement mode, for the two different particle sizes as observed experimentally. Furthermore, the model predicts a critical field lower than that given by the nDEP mechanism and much closer to the experimental results. This is particularly noticeable for the smallest particle size. Importantly, experiments show a much smoother transition from zero lateral displacement to the maximum deviation angle, mainly for the smaller particles. This is not predicted by the simulations, which show an abrupt transition between displacement or zig-zag. This sharp transition is expected from a fully deterministic behaviour of the particles. The smoothness observed experimentally is attributed to experimental artifacts not accounted for in the simulations, mostly the non-uniformity of the electric field magnitude across the channel caused by changes in the local conductivity near the electrodes [31].

Although the deviation angle defined by the DLD array is equal in both experiments and simulations, there is an observed difference in the maximum value of the deviation angle. This is simply due to the specific design of the experimental DLD devices (explained in [12]). The devices have a region near the electrode with zero pillar array offset where fully deflected particles concentrate. Particles in a displacement trajectory reach this region before they arrive at the end of the channel, and travel in a straight line with zero deviation. Since the experimental deviation angle is estimated from the total displacement at the end of the channel and the channel length, this leads to a smaller angle than that defined by the array geometry.

4.2. Low frequency behaviour: contributions of EP and CPEO

The numerical model was then used to analyse the contribution of the CPEO particle-wall interaction to the deviation with a low frequency electric field perpendicular to the flow. For this purpose, particle trajectories were simulated taking into account solely the influence of the EP oscillation or the influence of combination of EP and CPEO. Fig. 6 summarises the results for the deviation of 1 µm and 3 µm particles at 50 Hz and a v_0 measured at this frequency and 2.8 mS/m. It shows that the EP oscillation alone can induce deviation of particles via inelastic collision with the pillar walls. We hypothesize that the collisions limit the oscillating motion towards the posts giving a non-zero time average lateral displacement that is magnified after interaction with several posts. The symmetry of this mechanism is broken by the tilt angle of the DLD array, leading to a preferential direction in the post-particle interaction driven by the EP oscillation.

However, as shown in Fig. 6, the critical field is significantly reduced when the CPEO wall interaction is included in the simulations. Importantly, there was no deviation when only the CPEO wall-interaction is considered (ignoring the EP oscillation) for any of the two particles sizes, in the range of field amplitudes explored. Fig. 6a shows the low frequency deviation for two different particle sizes, demonstrating that the reduction in the critical field is more noticeable for the smallest particles. Fig. 6b shows how the deviation of the 3 µm diameter spheres depends on the frequency of the applied electric field. It shows that, as the frequency increases, the influence of the CPEO interaction becomes more prominent. At 50 Hz, the addition of CPEO decreases the critical field magnitude by ~5% whereas for 167 Hz the reduction is more than 30%. This implies that as frequency increases, the contribution of the EP oscillations decreases faster than the CPEO wall interaction.

Fig. 7 shows an example of how this mechanism works. It shows the trajectory of a 1 µm diameter rigid sphere in a DLD array under the influence of a 50 Hz field perpendicular to the flow for: (a) the EP force, (b) the CPEO wall-interaction and (c) combination of both. These simulations were done at a field of 43 kV/m, corresponding to the regime where the EP oscillation alone does not induce deviation, but only when combined with CPEO. Fig. 7a depicts how, when only the EP force is considered, the particles barely interact with the posts because of the distortion of the electric field lines around the insulating posts. When the CPEO wall interaction is the only mechanism (Fig. 7b), particles only pass near the posts for a small portion of their trajectories. Since the CPEO decays with distance to the wall squared, this interaction does not lead to a large change in the particle trajectory. When both mechanisms are combined (Fig. 7c), the particle oscillations along the field lines drive the particles near the post walls, maximising the effect of the CPEO particle-wall interaction leading to the induced particle deviation. These results lead to the conclusion that only when both mechanisms are combined, there is an accurate prediction of the observed experimental trends. Thus there is a non-linear dependence of the induced deviation with the electric field magnitude, a decline with the electric field frequency and the electrolyte conductivity and the lack of a direct relationship between the oscillation amplitude and the induced deviation.

4.3. Comparison between a parallel and a perpendicular field

Finally the particle trajectories were examined with the electric field applied parallel to the fluid flow. This configuration has been experimentally characterised by Tegenfeldt et al. [9,10,32]. They found very similar trends with nDEP dominating at high frequencies and/or high medium conductivities; the high frequency deviation can be fully explained by DEP. However, deviation at low frequencies is different, with the effect decreasing with the field frequency and electrolyte conductivity. Interestingly, they also showed that the particle surface charge was directly linked to the low frequency induced deviation [10]. Under the same conditions, particles with a higher surface charge had a reduced

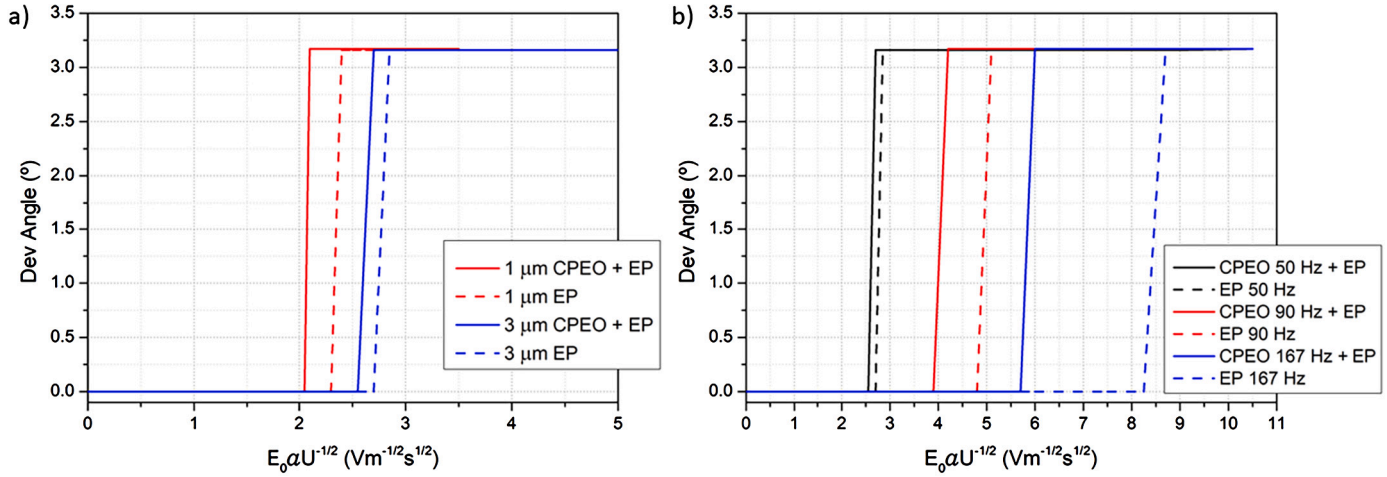

Fig. 6. Comparison of the deviation induced by EP oscillation only and EP oscillation combined with CPEO induced deviation. (a) Two different particle sizes at 50 Hz. (b) 3 µm diameter particles at different field frequencies.

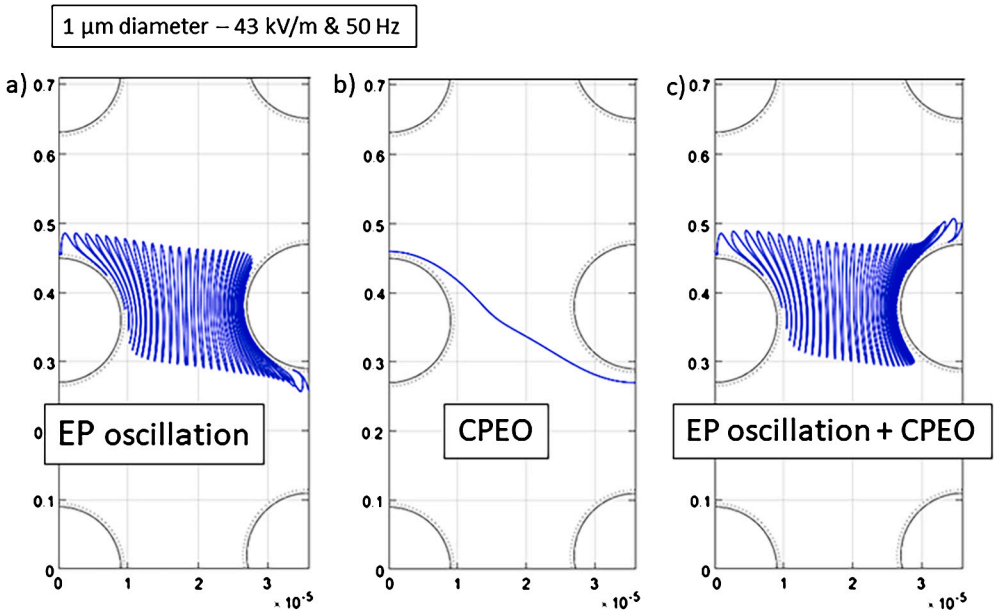

Fig. 7. Example of simulated trajectories of 1 µm diameter particle inside DLD devices with a low (50 Hz) frequency electric field perpendicular to the fluid flow. (a) Contribution only from electrophoretic oscillation. (b) Only CPEO contribution. (c) Combination of CPEO and EP oscillation.

critical electric field magnitude, i.e. they deviated for lower values of field strength. This matches the hypothesis that the low frequency deviation is dominated by a combination of CPEO and EP oscillation, since both mechanisms are stronger for a higher surface charge density. Also, in this case, the EP oscillation occurs in the direction of the fluid flow (along the field lines), so that this mechanism alone could not lead to an increased wall-particle interaction.

The simulations show that when the field is applied in the direction of fluid flow, there is no induced deviation when any of the two mechanisms, CPEO wall interaction or EP oscillation, is considered independently. Only when the two are combined does the electric field force the particles to switch to the displacement mode. In contrast to the perpendicular field, with the field parallel to the fluid flow, the EP oscillation takes place in the direction of the fluid streamlines and so does the inelastic post-particle interaction. As a result, the oscillations alone cannot produce the net displacement required to push particles across the separatrix streamline. Similar to the perpendicular case, when the CPEO acts independently, particles only spend a small fraction of time near the posts, so that the effects of the CPEO wall interaction are largely reduced. Only when the oscillating trajectories drive the particles back and forth near the post wall, does the CPEO effect accumulate forcing the particles to deviate.

Fig. 8 shows the simulation results at 50 Hz with the field applied in the direction of the fluid flow (as a function of electric field magnitude). The figure shows a comparison with the maximum nDEP induced deviation. For the 1 µm particles, there is a negligible difference between the critical field magnitude given by the nDEP mechanism and the low frequency induced deviation. However, for the bigger particles of 3 µm, there is a significant reduction in critical field magnitude for the low frequency mechanism. This figure also provides a comparison between the predicted low frequency deviation for an electric field applied perpendicular (⊥) and parallel (∥) to the fluid flow. The predicted deviation of the 3 µm spheres is approximately equal for both field orientations. Nevertheless, the critical field magnitude for the smaller 1 µm diameter particles is significantly lower for the perpendicular field. This result suggests that a perpendicular field is the optimal configuration to maximise the deviation of particles that are substantially smaller than the critical diameter [33].

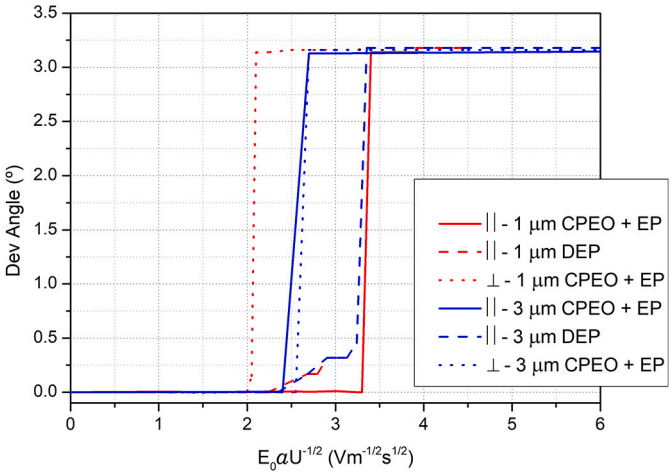

Fig. 8. Comparison between nDEP and low-frequency induced deviation for an electric field applied parallel to the fluid flow (‖) and the low-frequency deviation induced by an electric field perpendicular to the fluid flow (⊥). Note that, as in Fig. 5, the simulation results for the high-frequency deviation of 1 μm and 3 μm overlap.

5. Conclusions

In conclusion, these numerical simulations have provided a comprehensive understanding of the factors that govern the low-frequency electrokinetic-induced sorting of particles inside a microfluidic DLD channel. We have demonstrated that the CPEO wall-particle interaction combined with EP oscillation fully explains the deflection induced by low-frequency electric fields, with the simulations matching the experimentally observed trends. Note that electrothermal flows have been neglected, given that this phenomenon occurs at higher electrolyte conductivities.

By establishing a link between the recently reported CPEO mechanism and the low-frequency electrokinetic separation of particles in DLD devices, our model consolidates previous experimental and numerical results, completing the theoretical framework for a full understanding of the behaviour of electrokinetic-biased DLD particle separation systems. The implications of our findings are significant in the design and optimization of DLD devices for particle sorting and fractionation, when combined with electric fields, enabling particles significantly smaller than the critical diameter to be deflected and sorted. The simulations can be used to tailor the physical and electrical properties of the particles to achieve specific separation outcomes, and to optimize the post-array geometry, field frequency and conductivity of the solution to enhance separation efficiency.

CRediT authorship contribution statement

Víctor Calero: Conceptualization, Data curation, Formal analysis, Investigation, Methodology, Software, Validation, Visualization, Writing – original draft. **Raúl Fernández-Mateo:** Data curation, Formal analysis, Investigation, Methodology, Software, Validation, Writing – review & editing. **Hywel Morgan:** Formal analysis, Funding acquisition, Validation, Writing – review & editing. **Pablo García-Sánchez:** Conceptualization, Formal analysis, Methodology, Software, Supervision, Validation, Writing – review & editing. **Antonio Ramos:** Conceptualization, Formal analysis, Funding acquisition, Methodology, Supervision, Validation, Writing – review & editing.

Declaration of competing interest

The authors declare that they have no known competing financial interests or personal relationships that could have appeared to influence the work reported in this paper.

Data availability

The data that support the findings of this study are openly accessible in the University of Southampton repository available at https://doi.org/10.5258/SOTON/D2730.

Acknowledgements

P.G.S. and A.R. acknowledge Grant P20-00534 funded by Consejería de Economía, Conocimiento, Empresas y Universidad, Junta de Andalucía.

Appendix A. Supplementary material

Supplementary material related to this article can be found online at https://doi.org/10.1016/j.chroma.2023.464240.

References

[1] H. Cho, J. Kim, H. Song, K.Y. Sohn, M. Jeon, K.-H. Han, Analyst 143 (2018) 2936.
[2] H.W. Hou, M.E. Warkiani, B.L. Khoo, Z.R. Li, R.A. Soo, D.S.-W. Tan, W.-T. Lim, J. Han, A.A.S. Bhagat, C.T. Lim, Sci. Rep. 3 (2013) 1259.
[3] P. Ohlsson, M. Evander, K. Petersson, L. Mellhammar, A. Lehmusvuori, U. Karhunen, M. Soikkeli, T. Seppa, E. Tuunainen, A. Spangar, et al., Anal. Chem. 88 (2016) 9403.
[4] J.C. Contreras-Naranjo, H.-J. Wu, V.M. Ugaz, Lab Chip 17 (2017) 3558.
[5] K. Loutherback, J. D'Silva, L. Liu, A. Wu, R.H. Austin, J.C. Sturm, AIP Adv. 2 (2012) 042107.
[6] B.H. Wunsch, J.T. Smith, S.M. Gifford, C. Wang, M. Brink, R.L. Bruce, R.H. Austin, G. Stolovitzky, Y. Astier, Nat. Nanotechnol. 11 (2016) 936.
[7] J. McGrath, M. Jimenez, H. Bridle, Lab Chip 14 (2014) 4139.
[8] L.R. Huang, E.C. Cox, R.H. Austin, J.C. Sturm, Science 304 (2004) 987.
[9] J.P. Beech, P. Jönsson, J.O. Tegenfeldt, Lab Chip 9 (2009) 2698.
[10] B.D. Ho, J.P. Beech, J.O. Tegenfeldt, Micromachines 11 (2020) 1014.
[11] V. Calero, P. Garcia-Sanchez, C. Honrado, A. Ramos, H. Morgan, Lab Chip 19 (2019) 1386.
[12] V. Calero, P. Garcia-Sanchez, A. Ramos, H. Morgan, J. Chromatogr. A (2020) 461151.
[13] L. Liang, Y. Ai, J. Zhu, S. Qian, X. Xuan, J. Colloid Interface Sci. 347 (2010) 142.
[14] L. Liang, S. Qian, X. Xuan, J. Colloid Interface Sci. 350 (2010) 377.
[15] R. Fernandez-Mateo, V. Calero, H. Morgan, P. Garcia-Sanchez, A. Ramos, Phys. Rev. Lett. 128 (2022) 074501.
[16] R. Fernández-Mateo, P. García-Sánchez, V. Calero, H. Morgan, A. Ramos, J. Fluid Mech. 924 (2021).
[17] V. Calero, R. Fernández-Mateo, H. Morgan, P. García-Sánchez, A. Ramos, Phys. Rev. Appl. 15 (2021) 014047.
[18] J. Lyklema, Fundamentals of Interface and Colloid Science, Academic Press, Limited, 1995.
[19] H. Morgan, N.G. Green, AC Electrokinetics: Colloids and Nanoparticles, Research Studies Press Ltd., 2003.
[20] M. von Smoluchowski, Bull. Akad. Sci. Cracovie. 8 (1903) 182.
[21] N. Gamayunov, V. Murtsovkin, A. Dukhin, Colloid J. USSR 48 (1986) (Engl. Transl.), United States.
[22] J. Happel, H. Brenner, Low Reynolds Number Hydrodynamics: with Special Applications to Particulate Media, vol. 1, Springer Science & Business Media, 2012.
[23] E. Yariv, Proc. R. Soc. A, Math. Phys. Eng. Sci. 465 (2009) 709.
[24] J.R. Smart, D.T. Leighton Jr, Phys. Fluids A, Fluid Dyn. 3 (1991) 21.
[25] S.-C. Kim, B.H. Wunsch, H. Hu, J.T. Smith, R.H. Austin, G. Stolovitzky, Proc. Natl. Acad. Sci. 114 (2017) E5034.
[26] J.E. Flores-Mena, P. García-Sánchez, A. Ramos, Micromachines 14 (2022) 23.
[27] R.V. Davalos, G.J. McGraw, T.I. Wallow, A.M. Morales, K.L. Krafcik, Y. Fintschenko, E.B. Cummings, B.A. Simmons, Anal. Bioanal. Chem. 390 (2008) 847.
[28] M. Viefhues, S. Manchanda, T.-C. Chao, D. Anselmetti, J. Regtmeier, A. Ros, Anal. Bioanal. Chem. 401 (2011) 2113.
[29] R. Fernández-Mateo, P. García-Sánchez, V. Calero, A. Ramos, H. Morgan, Electrophoresis 43 (2022) 1259.
[30] R. Fernández-Mateo, P. García-Sánchez, V. Calero, A. Ramos, H. Morgan, Electrophoresis 43 (2022) 1259–1262.
[31] V. Calero, P. Garcia-Sanchez, A. Ramos, H. Morgan, Biomicrofluidics 13 (2019) 054110.
[32] B.D. Ho, J.P. Beech, J.O. Tegenfeldt, Micromachines 12 (2021).
[33] R.J. Gillams, V. Calero, R. Fernandez-Mateo, H. Morgan, Lab Chip 22 (2022) 3869.